Corticofugal feedback can reduce the visual latency of responses to antagonistic stimuli

J. Köhn, F. Wörgötter

Institut für Physiologie Abteilung Neurophysiologie, Ruhr-Universität, D-44780 Bochum, Germany

Abstract. A biophysically realistical model of the primary visual pathway is designed, including feedback connections from the visual cortex to the lateral geniculate nucleus (LGN) – the so-called corticofugal pathway. The model comprises up to 10 000 retina and LGN cells divided into the ON and the OFF pathway according to their contrast response characteristics. An additional 6000 cortical simple cells are modeled. Apart from the direct excitatory afferent pathway we include strong mutual inhibition between the ON and the OFF subsystems. In addition, we propose a novel type of paradoxical corticofugal connection pattern which links ON dominated cortical simple cells to OFF-center LGN cells and vice versa. In accordance with physiological findings these connections are weakly excitatory and do not interfere with the steady-state responses to constant illumination, because during the steady-state inhibition arising from the active pathway effectively silences the non-stimulated pathway. At the moment of a contrast reversal the effect of the paradoxical connection pattern comes into play and the depolarization of the previously silent channel is accelerated, leading to a latency reduction of up to 4 ms using moderate synaptic weights. With increased weights reductions of more than 10 ms can be achieved. We introduce different synaptic characteristics for the feedback (AMPA, NMDA, AMPA + NMDA) and show that the strongest latency reduction is obtained for a combination of the membrane channels (i.e., AMPA + NMDA). The effect of the proposed paradoxical connection pattern is self-regulating; because the levels of inhibition and paradoxical excitation are always driven by the same inputs (strong inhibition is counterbalanced by a stronger paradoxical excitation and vice versa). In addition, the latency reduction for a contrast inversion which ends at a small absolute contrast level (small contrast step) is stronger than the reduction for an inversion with large final contrast (large contrast step). This leads to a more pronounced reduction in the reaction times for weak stimuli. Thus, reaction time differences for different contrast steps are smoothed out.

Correspondence to: F. Wörgötter

1 Introduction

A prominent feature of the primary visual pathway is the massive feedback connection structure which arises between the visual cortex (area 17, V1) and the lateral geniculate nucleus (LGN) in the thalamus. Up to 45% of the synapses on LGN cells have their origin in the cortex, whereas the direct retinal input constitutes only about 10–15% (for a review see Sherman and Koch 1986). So far the only way to assess the influence of these connections experimentally is to inactivate the cortex during electrophysiological recording of LGN cell behavior. However, only minor effects, were found in most of the older studies which applied this technique, the majority of which resulted in a rather global depression of LGN cell activity (Kalil and Chase 1970; Richard et al. 1975; Baker and Malpeli 1977; Geisert et al. 1981). Normally LGN cells continue to fire as long as the stimulus is presented and little adaptation occurs. This sustained response is substantially reduced during cortical inactivation and the cell response decays to zero rather fast. A more specific effect in the spatial domain was evidenced by Murphy and Sillito (1987), who have shown that the corticofugal connections can have an influence on the length tuning of LGN cells.

More recently McClurkin et al. (1994) have demonstrated that the flow of visual information is enhanced as a consequence of corticofugal feedback. In particular, they found that the temporal distribution of spikes is altered during cortical cooling. Along the same lines Sillito et al. (1994) showed that LGN cells fail to synchronize as soon as the cortex is removed. These two findings indicate that the corticofugal connections could predominantly influence time-dependent aspects of cell behavior in the LGN.

The latency to response can be regarded as one of the most basic temporal effects which occurs in every sensory

neuron. The time delay (latency) until the first action potential is elicited usually depends on the stimulus intensity. Strong stimuli cause fast responses, while it takes longer for a cell to react to a weak stimulus. If a system is required to react immediately, long response latencies are undesirable. Also, strongly varying latencies should be avoided to make the reaction time less dependent on the stimulus intensity.

In the retina and LGN subgroups of cells exist that respond to a positive (bright) contrast or a positive contrast change (ON-center cells), while cells of another subgroup require dark contrasts (OFF-center cells: for a review see Casagrande and Norton 1991). The two pathways remain separate even at the level of cortical simple cells, which contain adjacent nonoverlapping subfields that respond either to bright or to dark stimuli (Hubel and Wiesel 1962). Moreover, it is very likely that the two subsystems mutually inhibit each other (push-pull connection structure), which subserves the purpose of improving the linearity of spatial summation (Glezer et al. 1980; Palmer and Davis 1981; Ferster 1988; Tolhurst and Dean 1990).

In a visual environment transitions between bright and dark stimuli occur rather often as the consequence of object or eye movements. If, for example, at the same retinal location, a bright stimulus is followed by a dark stimulus, the ON system stops responding and the OFF system takes over. As a result of the bright stimulus which was present before the contrast change, the OFF system has to leave the state of inhibition before its response can set in. This, however, will take time, particularly if the new stimulus has only a small absolute contrast value, which leads to only a weak retinal excitation.

In this theoretical study we propose a novel type of connection structure from the visual cortex to the LGN which is designed so that the visual latencies to such antagonistic stimuli are reduced in LGN and cortex.

To achieve the desired acceleration of a cell response to a contrast change in the opposite direction we propose a paradoxical corticofugal connection structure which links the ON to the OFF subsystems by weak excitatory connections and vice versa. Figure 1 shows the wiring diagram. The LGN cells receive input from ON- (1, right) and OFF-center ganglion cells (2, left) in the retina and both inputs come from exactly the same projection areas in the visual field. Thus, the locations of the receptive fields in retina, LGN and cortex are identical. The LGN cells in turn project to cortical simple cells (5, 6). For the sake of simplicity we assume for now that these 'simple cells' contain only one subfield, i.e., their contrast sensitivity resembles those of the LGN cells. This limitation can be dropped (see Sect. 4). At the level of LGN (3, 4) and cortex (7, 8) mutual inhibition between the ON and OFF subsystems is implemented. The novel connection structure that we propose excitatorily connects the cortical 'ON' cell to the LGN OFF cell (9) and vice versa (10).

Let us assume constant illumination with a bright stimulus. During this steady-state the low level of excitation coming from the paradoxical connection (9) does not induce changes in cell behavior of the LGN OFF cell,
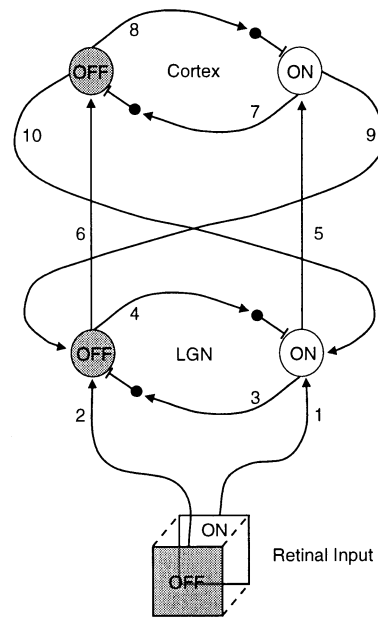
Fig. 1. Connection scheme used for the simulations

which remains inhibited by the much stronger direct LGN inhibitory connections. With a contrast change in the opposite direction (bright turns to dark), the small amount of cortically induced excitation at the OFF system persists for a short time after the moment of the contrast change. Almost at the same time the first input spikes from the retina arrive. Consequently both simultaneously active excitatory inputs will lead to a faster response (reduced latency) of the LGN cell as compared with a situation where the LGN cell is depolarized by the effect of the retinal input alone.

In the following sections we will describe a biophysically realistical simulation of the proposed circuit (Fig. 1). Different types of synapses (AMPA vs NMDA) will be introduced for the corticofugal connections. We will show that a considerable latency reduction can be achieved by the paradoxical corticofugal connections. This effect is most strongly pronounced for feedback using AMPA synapses, while NMDA synapses by themselves do not contribute significantly.

2 Description of the model

2.1 General layout: connection structure

The simulator that we used exists in two versions: a massive parallel version with about 16 000 neurons, running on a supercomputer (Connection Machine CM2), and a serial version of a few hundred neurons running on a workstation. The basic version of the simulator has been described in detail by Wörgötter and Koch (1991) and by Brettle and Niebur (1994). Therefore, in the following we will only briefly summarize the model. We will, however, give all the details about model changes which affect the basic setup.

The retina is simulated as a preprocessing step to generate the first spikes in the system. In the original version the retina model contains difference-of-Gaussian receptive field filters with different polariy to mimic ON- and OFF-center ganglion cells (Wörgötter and Koch 1991). There the model represented a two-dimensional patch of 5×5 deg of the primary visual pathway. In the current study we entirely omit the spatial structure of the model and focus only on the temporal characteristics. This is essentially equivalent to simulating small dots in the center of a retina cell's receptive field. To get the spike train, normally a convolution of such a stimulus time-function with the receptive fields filter has to be computed and spikes are then elicited by a stochastic process. Originally this was a Poisson process (Wörgötter and Koch 1991). Retinal activity elicited by a spatially distinct stimulus (e.g., small dot), however, is better reflected by a gamma inter-spike interval distribution, which in most cases cannot be distinguished in shape from a simple Gaussian (Troy and Robson 1992). Therefore, for the current simulations we resorted to directly mapping a Gaussian probability function to the output of an individual retina cell representing its inter-spike interval distribution. The complete calculation of the spatial convolution between receptive field filter and dot-stimulus was only performed to check the validity of this approximation and to define the parameters of the Gaussian. The standard deviation of the Gaussian inter-spike interval distribution was 4 ms; the mean value was contrast dependent. Eight milliseconds were assumed for 100% contrast (Funke and Wörgötter 1995) and this value was increased using a sigmoidal characteristic to a maximum of 24 ms for the lowest contrast used (5%).

The cell model, which implements the properties of cells along the visual pathway, including LGN and cortex cells, is based on a so-called improved integrate-and-fire model. The main equations and parameters of the simulations and the implementation of the NMDA channels are described in Sect. 2.2.

In the next step the ganglion cell spikes are projected onto two LGN cell groups, each projection terminating on four LGN cells. One of these groups represents a cluster of LGN ON cells; the other represents LGN OFF cells; both receive ganglion cell spikes from the same retinal subfield. Each of the two cell groups is connected to one cortical cell, representing an ON and an OFF cortex cell, respectively. Thus, we do not model several subfields in the cortex cells. Restrictions imposed by this model setup will be elaborated on in Sect. 4.

Each LGN cell of one cluster inhibits two LGN cells in the other cluster. This strong mutual inhibition between the ON and OFF pathways ensures that if one pathway is active, the other is silent. A similar mutual inhibitory connection scheme is introduced in the cortex. The paradoxical pathway is designed by connections from the cortex cell of one pathway, to all four LGN cells of the other pathway. For detailed information about conductances and synaptic weights, see Sect. 2.3.

2.2 Characteristics of neurons and membrane channels

The improved integrate-and-fire neurons are described by the following differential equation for the membrane potential:

$$
C_i \frac{dV_i}{dt} = \sum_{j=1}^{k} g_{i,j,\text{exc}}(t)(E_\text{exc} - V_i)
$$

$$
+ \sum_{j=1}^{l} g_{i,j,\text{inh}}(t)(E_\text{inh} - V_i)
$$

$$
+ g_\text{leak}(E_\text{leak} - V_i) + g_{i,\text{AHP}}(t)(E_\text{AHP} - V_i) \quad (1)
$$

where C_i is the membrane capacity of cell i, V_i is the membrane potential of cell i, $g_{i,j,\text{exc/inh}}(t)$ is the conductance of an excitatory/inhibitory channel from presynaptic cell j to postsynaptic cell i at time t, g_leak is the leakage conductance, $g_{i,\text{AHP}}(t)$ is the conductance of the after-hyperpolarization (AHP) of cell i, $E_\text{exc/inh}$ is the excitatory/inhibitory reversal potential, E_leak is the resting potential, and E_AHP is the reversal potential of the after-hyperpolarization. The solution of this differential equation is calculated for each cell during the simulation using a (Fourth order) Runge-Kutta method.

Excitatory synaptic inputs (g_exc) are implemented in the model in two versions: (i) AMPA (alpha-amino-3-hydroxy-5-methyl-4-isoxazole proprionic acid) channels, which are not voltage dependent, and (ii) NMDA (N-methyl-D-aspartate) channels, which are voltage dependent. The time course of the conductance of an AMPA channel, an inhibitory channel and the after-hyperpolarization is that of a simple alpha-function (for parameters see Tables 1, 2):

$$
g_\text{AMPA} = \hat{g}_A \frac{e}{\tau} t e^{-t/\tau} \quad (2)
$$

where $\hat{g}_A$ is the peak conductance of the AMPA channel and τ is the time constant of the AMPA channel (1 ms).

All computations are performed in discrete time steps T of 0.1 ms. We need to solve the convolution of the input function $I_i(t)$ [see (3)], which is a temporal sequence of delta impulses (spikes), with (2). To increase the speed of computation, the $\mathscr{Z}$-transform is used (Doetsch 1967; Oppenheim and Schafer 1975):

$$
I_i(t) =
$$

$$
\begin{cases} \delta(t) & \text{if } V_i(t) > V_i^\text{threshold} \text{ and } I_i(t') = 0 \forall t' > t - \tau_r \\ 0 & \text{else} \end{cases} \quad (3)
$$

where $V_i^\text{threshold}$ is the threshold for the action potential and τ_r is the refractory period.

The result of the $\mathscr{Z}$-transform, the convolution and the retransform is shown in (4). It can be seen that only two time steps from the past are necessary to compute the actual conductance of one membrane channel of a cell. These are $y((n-1)T)$ and $y((n-2)T)$, the conductance values of the last and the last but one time step T. Thus, the $\mathscr{Z}$-transform saves a considerable amount of computational effort as compared with a conventional

convolving algorithm, while still being an exact solution of the convolution.

$$y(nT) = T \cdot \hat{g}_A \cdot e^{-T/\tau} x((n-1)T)$$
$$+ 2e^{-T/\tau} y((n-1)T) - e^{-2T/\tau} y((n-2)T) \quad (4)$$

where T is the time step, $y(nT)$ is the conductance at time nT, $y((n-1)T$ is the conductance one time step previously, $y((n-2)T$ is the conductance two time steps previously, and $x(nT-)$ is the weighted input during the last time step.

The new feature of this simulator which distinguishes it from previous versions is the implementation of NMDA channels, known by their slow channel characteristic and their dependence on the membrane potential. We used (5) to describe the properties of this special channel type. This equation, or a similar one, has also been used by others (Mel 1992; Bernard et al. 1994) and takes into account the large time constant as well as the voltage dependence.

$$g_{NMDA} = \hat{g}_N \frac{e^{-t/\tau_1} - e^{-t/\tau_2}}{1 + \eta[Mg^{2+}]e^{-(\gamma V_m)}} \quad (5)$$

where $\hat{g}_N$ is the peak conductance of the NMDA channel, τ_1, τ_2 are the first and second time constants of the AMPA channel ($\tau_1 = 80$ ms, $\tau_2 = 0.66$ ms), $[Mg^{2+}]$ is the magnesium concentration in $[mM]^{-1}$, η is 0.33 mM^{-1}, γ is 0.06/mV, and V_m is the membrane potential in mV.

Salvaging the advantage of the necessity for very little history information, we also use the $\mathscr{Z}$-transform to determine the convolution of the NMDA channel equation with the delta-pulse-input function $I_i(t)$ (for details on the derivation see the Appendix). The final result is

$$y(nT) = \frac{1}{1 + \eta[Mg^{2+}]e^{-\gamma V_m}}$$
$$\cdot (\hat{g}_N \cdot (e^{-T/\tau_1} - e^{-T/\tau_2}) \cdot x((n-1)T)$$
$$+ (e^{-T/\tau_1} - e^{-T/\tau_2}) \cdot y((n-1)T)$$
$$- (e^{-T/\tau_1} \cdot e^{-T/\tau_2}) \cdot y((n-2)T)) \quad (6)$$

where T is the time step, $y(nT)$ is the conductance at time nT, $y((n-1)T$ is the conductance one time step previously, $y((n-2)T$ is the conductance two time steps previously, and $x(nT-)$ is the weighted input during the last time step.

To test the correct implementation of the channel behavior and to compare it with real measured data, single and multiple inputs were simulated at a single AMPA or NMDA channel. In Fig. 2 the conductances and the membrane potentials are plotted against time. Figure 2b shows the conductance change of an AMPA and of an NMDA channel to a single incoming spike (Fig. 2a). The reaction of the AMPA channel is very short, as opposed to the reaction of an NMDA channel, which has a smaller peak but a duration of up to a few hundreds of milliseconds. As an additional estimate of the behavior we show the time course of the membrane potential (Fig. 2c) for a single spike. The two relevant variables time-to-peak $t_{\text{to-peak}}$ and time-to-half-decay-
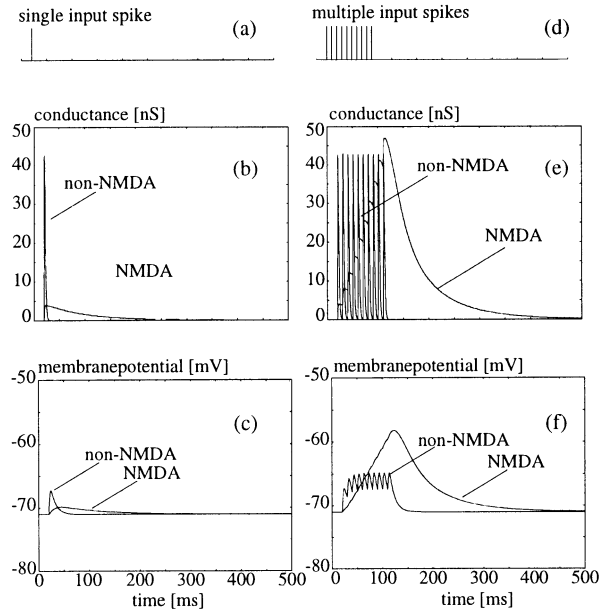
Fig. 2a–f. Verification of the channel characteristics. **a** The single input spike, which causes a depolarization of the postsynaptic membrane. **b** The conductances of both (AMPA and NMDA) ion channels; **c** the corresponding membrane potential. **d–f**. Similar diagrams for multiple input spikes (100 Hz)

from-peak $t_{1/2\text{peak}}$ are 21.2 ms and 49.3 ms, respectively. The values are similar to those measured by Singer and Artola (1990) ($t_{\text{to-peak}}$, 25.0 ms; $t_{1/2\text{peak}}$ 56.0 ms), and Jones and Baughman (1988) ($t_{\text{to-peak}}$, 19.6 ms; $t_{1/2\text{peak}}$ 51.4 ms).

To demonstrate the reaction to an incoming spike train the input shown in Fig. 2d with 10 spikes and a frequency of 100 Hz is chosen. As expected, the two channels react in a different way. The time course of conductance changes for the AMPA channel (Fig. 2e) is just a replica of that for a single input spike (Fig. 2c), because the time constant of the AMPA channel is smaller than the input frequency. The NMDA channel with its long lasting behavior has an integrative effect on the input and sums the input over a long period (Fig. 2e). Figure 2f shows the same effect for the membrane potential, where only a small integrative effect can be observed for the AMPA channel and a much stronger one for the NMDA channel. In general, these plots show that the equations simulate the neuronal characteristics to a sufficiently realistic degree.

2.3 Parameter settings

Tables 1 and 2 summarize the parameters used during all simulations. Table 1 gives the parameters for the main differential equation (1).

In Table 2 the connection parameters are listed. All paths between different cells have four specific parameters. *Weight* describes the synaptic weights between two cells. The actual connection impact essentially relies on the product of *weight* and *peak conductance* of the channel. The different reversal potentials for excitatory AMPA, excitatory NMDA and inhibitory paths are

Table 1. The main parameters of the simulated neurons

Symbol	Parameter	Value
C	Capacity	1 nF for LGN and 2 nF for cortex cells
g_{leak}	Leakage conductance	0.1 μS for LGN and 0.2 μS for cortex
E_{leak}	Leakage reversal potential	-71 mV
τ_{AHP}	Time constant of after-hyperpolarization	1 ms
V_{AHP}	Reversal potential of after-hyperpolarization	-91 mV
g_{AHP}	Peak conductance of after-hyperpolarization	0.59 μS
w_{AHP}	Synaptic weight of after-hyperpolarization	50

Table 2. Overview of the important parameters for the different connections

Connection	Weight	Peak conductance (nS)	Reversal potential (mV)	Axonal delay (ms)
Retina → LGN	10	100	20	0
LGN-ON → LGN-OFF	50	300	-91	2
LGN-OFF → LGN-ON	50	300	-91	2
LGN → cortex	3	100	20	3
Intra-cortex	50	300	-91	2
Feedback	$0 \to 20$	AMPA 50	20	5
		NMDA 50	0	5

shown in column 4. Other important potentials are the resting potential of -71 mV and the fire threshold of -40 mV. The connection parameters *weight* and *axonal delay* are Gaussian distributed with a small sigma.

3 Results

Figure 3 shows the latency reduction that can be achieved with the paradoxical connections for different synaptic weights of the feedback. A comparison is made between no-feedback connections and feedback connections with AMPA, NMDA or AMPA + NMDA channels. It should be noted that the diagram only shows spike propagation latencies from the retinal ganglion cells to the LGN (or cortex). The true latencies in the visual system also include delays which arise as a consequence of electrochemical processes at the photoreceptors and the electronic network (bipolar, horizontal and amacrine cells) in the retina. This additional delay, however, is contrast dependent but additive and real latencies for medium contrasts are about 30–40 ms (Bolz et al. 1982) – longer than those which are produced in our network. The stimulus consists of a contrast step at t_0 from 100% to -100% contrast. Thus, the ON system is active before and the OFF system after the step. The retinal inter-spike interval distribution used as input to the system has a Gaussian shape (inset) with mean interval between two spikes of 8 ms. The occurrence time of the first spike after the step is taken as measure of the visual latency and is plotted against the synaptic weight of the paradoxical connections.

Standard deviation increases linearly in LGN and cortex. The initial value is identical to the standard deviation of the Gaussian input distribution. Maximum stan-
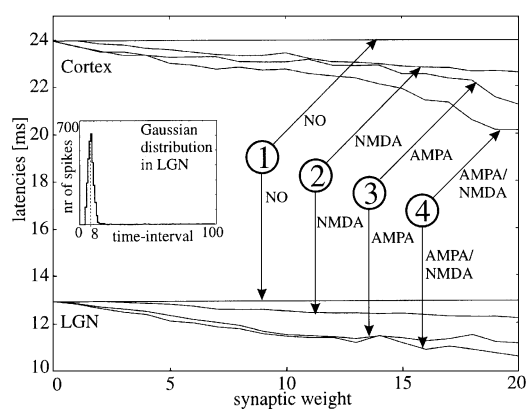
Fig. 3. Latency in LGN and cortex in response to alternating maximal contrast stimulation. The *inset* shows the inter-spike-interval distribution of the LGN. The mean interval length is about 8 ms. The *main part* of the diagram shows the results for a contrast input alternating between -100% and 100%. The latencies between the moment of the contrast change and the first spike in the LGN (*bottom*) or the cortex (*top*), respectively, are plotted against the synaptic weight of the feedback connection. Different combinations of synaptic channels have been used for the feedback connections. The latency obtained without feedback (*1*) is shown as a *straight line*

dard deviations are observed for the highest synaptic weight (20) in the AMPA/NMDA curve and are 1.75 ms larger in the LGN than the initial standard deviation of the input. In the cortex this effect is slightly amplified.

In all cases the synaptic weights of the feedback connections are such that no spikes are elicited during the wrong stimulus contrast because of the much stronger inhibition. With *no feedback* only one data point obtains, but this point was plotted as a straight line parallel to the *x*-axis for graphical reasons. Curves are

plotted for LGN and cortical cells. It can be seen that the latency reduction in the cortex can reach about 4 ms for the maximal synaptic weight. In the LGN the effect is much weaker with a maximum of 2 ms. The relative strength of the synaptic weights for the paradoxical connections can still be regarded as rather weak, and with larger weights we get a latency reduction of more than 10 ms in the cortex. The strongest effect always obtains for a combination of AMPA and NMDA channels at the feedback synapses, but the NMDA channel by itself leads only to a rather small effect, because the cells are hyperpolarized by inhibition during the wrong stimulus and the dynamic of the channel equation (5) simulates the blockage of the NMDA channels by magnesium ions during hyperpolarization.

A more intuitive understanding of the underlying process for latency reduction can be achieved through an analysis of the conductance changes at the different synapses (Fig. 4a–c). Due to the propagation delay between retina and LGN the first retina spikes arrive at the LGN cell about 6 ms after the contrast change (Fig. 4a). The intra-LGN inhibition drops (Fig. 4b) but persists for a short time after the contrast change, as the consequence of the axonal delay of the inhibitory connections. A similar but longer-lasting effect is observed for the corticofugal feedback loop (connection 2–6–10 in Fig. 1) and the last conductance peak occurs after 8 ms (Fig. 4c).

This conductance peak coincides with the incoming retinal activity and depolarizes the membrane of the LGN cell faster than without feedback (Fig. 4d), leading to a reduced response latency (reduction ≈ 2 ms). This effect is propagated and temporally amplified in the cortex, which leads to an even greater latency reduction there. Note that this explanation describes the general
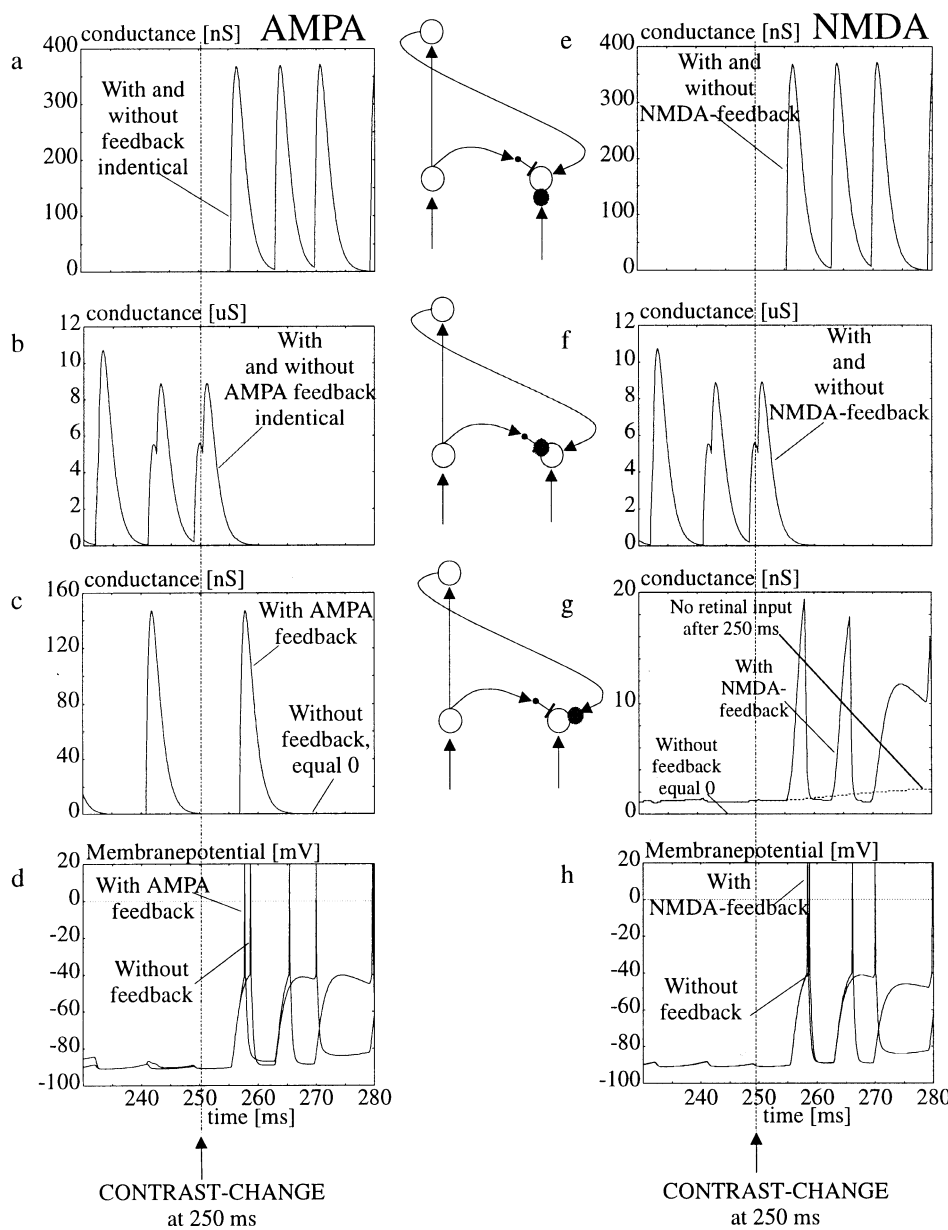
Fig. 4a–h. Membrane characteristics for the different channels during a contrast change. Contrast is changed at 250 ms, emphasized with a *dotted line*. a–d The time courses for an LGN ON cell with and without AMPA feedback; e–h for the same LGN ON cell with and without NMDA feedback from the cortex. a, e The retinal synapse(s); b, f the inhibitory intra-LGN synapse(s); c, g the feedback synapse(s) originating from the antagonistic cortex cell. d, h The resulting membrane potential of the LGN cell. In the connection diagrams in the *centre* the *black disc* enhances that particular synapse of which the conductance is plotted

effect of latency reduction. However, due to the convergence pattern in the model a *direct* temporal relation between any one pulse shown in one panel of Fig. 4 and any other pulse of another panel cannot be inferred.

If the AMPA channel which was used in the simulations of Fig. 4a–d is exchanged for an NMDA channel the latency reduction is much less (< 1 ms; Fig. 4h). Due to the long time constant of the NMDA characteristic [see (5) and Fig. 2], however, multiple conductance peaks occur (Fig. 4g). In fact, the occurrence of spikes which depolarize the membrane potential in the LGN followed by the after-hyperpolarization drives the NMDA conductance up and down. The envelope curve (dashed line) would reflect the behavior of the NMDA conductance without interspersed retinally induced spikes. As expected, curves Fig. 4e, f are identical to Fig. 4a, b.

So far we have concentrated only on single contrast steps between $\pm 100\%$. This is a situation which rarely occurs in a realistic visual environment. Generically all kinds of upward and downward contrast steps with and without sign inversion are to be expected following object or eye movements. Figure 5a shows an example trace of such a contrast time function, which we have used for another set of simulations. Contrast changes without sign inversion will lead to a change in the firing rate of an already active cell and the paradoxical connections do not have any effect. Thus, an evaluation of visual latency is only possible if the cells under investigation are silent and then – after the contrast change – start to fire. Therefore, only contrast changes with sign inversion were used to measure the resulting latencies.

In Fig. 5b, e we have plotted the latency in the cortex in a three-dimensional diagram, where one axis reflects the contrast at time T_n and the other axis the contrast at time T_{n+1}. Results from the ON and the OFF cells are combined in one diagram and each point on the surface is the averaged result from 50 contrast changes. As expected, long latencies occur for small absolute contrasts at T_{n+1}. The contrast before the change (i.e., at T_n) does not have any influence on the response in the case of no
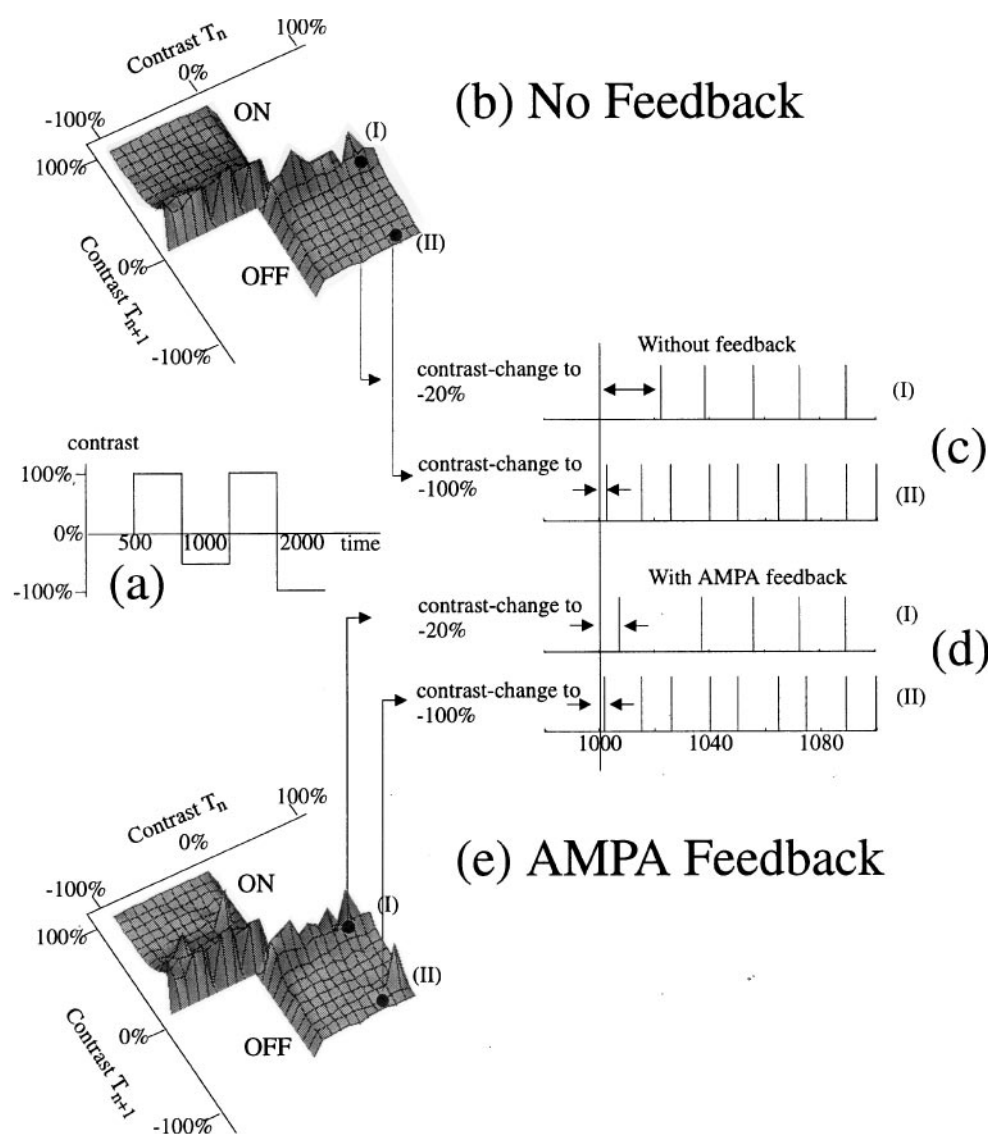
Fig. 5a–e. Response of the system to stochastic contrast changes: **a** The time course of a stochastic contrast change. Only contrast changes with a sign inversion have been used. **b, e** The resulting latencies with (**e**) and without (**b**) AMPA feedback, plotted with respect to the contrast *before* (at T_n) and that *after* the change (at T_{n+1}). Maximum peak height in **b** is 53.4 ms, in **e** 59.1 ms. **c, d** Two example spike trains for a low-contrast change to 20% (**c** I, **d** I) and a large contrast change to 100% (**c**, II, **d** II)

feedback (Fig. 5), and the variation in the surface along this direction is due only to statistical fluctuations. Example spike trains for two points on the surface with identical T_n are depicted in Fig. 5c. A change to a larger absolute contrast (c, II) results in a shorter latency and a higher firing rate than a change to a smaller contrast (c, I). The same two spike trains are shown in Fig. 5d for a simulation with an AMPA feedback loop. The latency is reduced in both traces as compared with Fig. 5c, but the absolute reduction is much more pronounced in the top trace, which represents the response to the small contrast change. Thus, the feedback loop has a tendency to level out the latency *differences* between large and small contrast steps. The firing rate does not change after including the feedback loop.

Figure 5e shows the whole diagram of latencies which are obtained with an AMPA feedback loop. The surface looks similar to that in Fig. 5b, but the subtraction of Fig. 5e from Fig. 5b (see Fig. 6) clearly shows the differences.

In Fig. 6 diagrams for the latency differences between simulations without and with feed backs are shown.

Thus, these diagrams can be directly interpreted as the latency reduction achieved by the paradoxical connections. When fixing the T_n value, curves obtain which show a rather monotonic increase towards small values of T_{n+1}. This means that in general the latency reduction is larger for a contrast step which leads to a small value of T_{n+1} (i.e., the new contrast value is small), as was already exemplified by Fig. 5b, e. When fixing the value for T_{n+1} the curves increase with increasing values of T_n. This is to be expected because only for high values of T_n does a strong influence of the paradoxical connections arise.

4 Discussion

On the basis of functional considerations, we have proposed in this theoretical study a hypothetical connection structure for the corticofugal pathway. The central idea behind this scheme was to reduce the response latencies in the case of a contrast change by means of paradoxical excitatory connections linking the two antagonistic
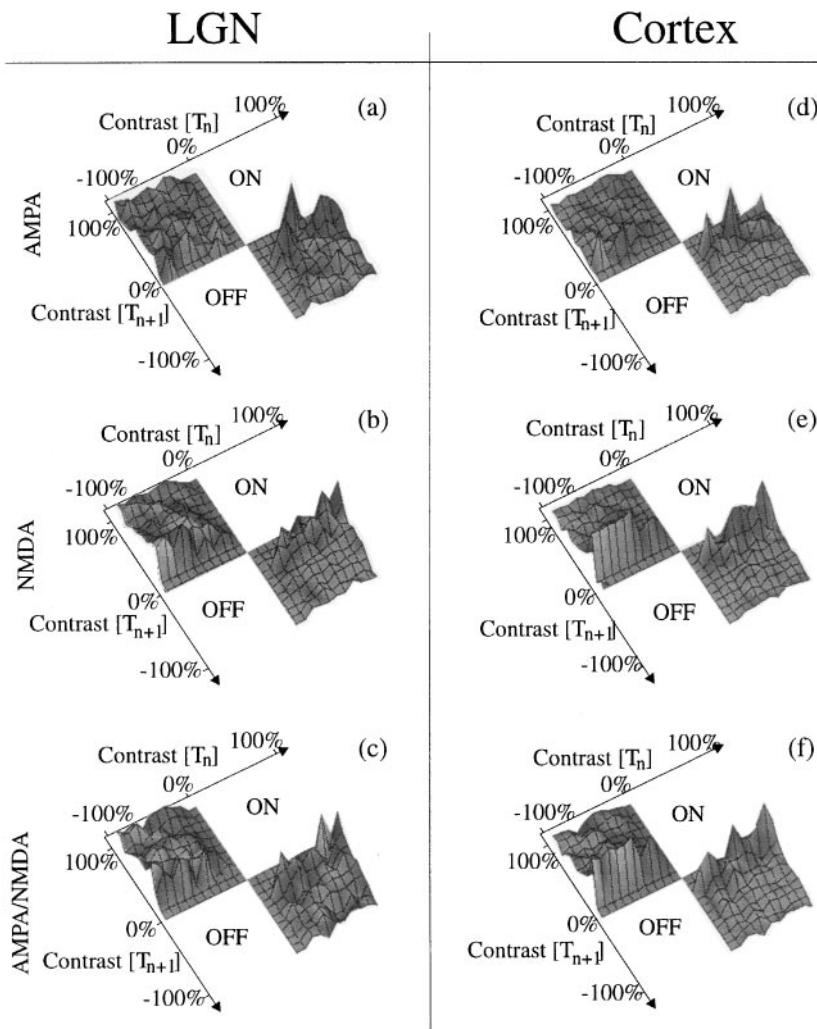
Fig. 6a–f. Latency reduction following stochastic contrast changes. The diagrams show the total reduction of the latencies subtracting the results obtained with and without feedback from each other. **a** The result for AMPA feedback; **b** for NMDA feedback; **c** for the combined AMPA and NMDA channel types for an LGN cell. **d–f** Results for a cortex cell. Maximum peak heights in the diagrams are: **a** 13.0 ms, **b** 32.4 ms, **c** 9.7 ms, **d** 25.8 ms, **e** 12.6 ms, **f** 27.6 ms

subsystems. The effect of latency reduction is achieved as the result of the loop duration from LGN to cortex and back which allows the paradoxical excitation to persist for a short time after the actual contrast change. Thus, two depolarizing inputs arrive at the LGN cell after the stimulus is reversed: one from the retina and one from the cortex via paradoxical connections. Consequently the depolarization is faster than in the case of only a retinal input. While this hypothetical idea and its advantages seem to be clear enough in the following section, we need to discuss the physiological limitations of our modeling approach.

The proposed connection structure is able to reduce that part of the visual latency which arises as the consequence of the axonal delay and the delay-to-threshold, which has to be reached by the depolarizing somatic currents before the cell starts to fire. Visual latencies, however, arise from several effects and the aforementioned delays are only one part which contributes to the total delay. Due to the structure of the model, which does not contain the retinal network, electrochemical processes in the retina are entirely omitted. In fact, the hyper- and depolarizing effects at retinal photoreceptors and the other parts of the retinal network constitute a major proportion of the visual latency (Levick 1973; Bolz et al. 1982). This, however, would mainly lead to an additive effect so that an additional contrast-dependent retinal latency would have to be added to each data point in the curves.

In general, our mechanism dwells on the temporal summation of the corticofugal excitation with another depolarizing signal, which in our case comes from the retina. In the LGN a release of inhibition can also trigger a low-threshold calcium spike, elicited as the consequence of voltage-dependent calcium currents (Llinas and Jahnsen 1982; Jahnsen and Llinas 1984). While this mechanism was not implemented in the model, it could be another source for the primary depolarization. The actual source of the depolarization, however, is not crucial as long as primary and corticofugally induced depolarization occur almost simultaneously.

In addition, we assume there are excitatory connections from the cortex to the LGN and that these connections have only a weak influence. It is almost certain that all corticofugal connections are excitatory (Baughman and Gilbert 1980; Montero 1994) and several reports show that only about 30% of the corticofugal connections terminate on inhibitory interneurons in the LGN (Montero 1991). Furthermore, all studies so far indicate that the corticofugal connections exert only a weak influence on the LGN cells (Kalil and Chase 1970; Richard et al. 1975; Baker and Malpeli 1977; Geisert et al. 1981), which might be due to the fact that they mostly terminate on the distal dendrites (Sherman and Koch 1986; Montero 1991).

In the model we have assumed that the cortical cells contain only one (either ON or OFF) subfield. For cortical simple cells this assumption does not hold and they consist sometimes of more than five subfields (Jones and Palmer 1987). In many situations it is sufficient to describe the receptive field of a simple cell by a two-dimen-

sional Gabor function, and Jones and Palmer (1987) have shown that almost all simple cell receptive fields show a significant deviation from a purely odd symmetrical Gabor function. Thus, almost all of them contain one *dominant* subfield, and in many cases this dominant subfield is so strongly pronounced that the responses from the other subfields play only a minor role. Therefore, our restriction to model cortical cells with only one subfield seems to be justified to some degree. There is, however, also another line of reasoning which can be used to solve this problem. Our model was designed such that specific paradoxical connections would facilitate the response to a contrast reversal. A latency reduction could, however, also be achieved by just a general nonspecific and weakly excitatory connection pattern arising from the cortex which converges onto LGN cells regardless of their ON-OFF polarity. Given such a nonspecific wiring pattern, let us assume a bright stimulus which excites the ON subsystem in the LGN. Due to the nonspecific and weak back-projections from the cortex, which would also converge onto the ON cells, the response would be enhanced, leading to a slightly increased firing rate in LGN and cortex. The OFF subsystem in the LGN, however, would still be subjected to the rather strong lateral inhibition. Only at the moment of contrast reversal would the weak corticofugal excitation come to life and a latency reduction occur in much the same way as for our connection pattern. Thus, for such a nonspecific connectivity pattern no more requirements are necessary concerning the structure of the receptive fields of the cortical cells. Nothing is known about the actual functionally guided connectivity of the corticofugal feedback. Our proposal of paradoxical corticofugal connections is rather specific, but it might well be that this assumption does not hold while the latency reduction due to nonspecific weakly excitatory corticofugal feedback still functions.

A central advantage of the proposed connection diagram, however, is its 'self-regulating' property in the sense that if the contrast is low, then the inhibition to the other subsystem is weak and the influence of the paradoxical connections is also weak. On the other hand, if the contrast is high, inhibition is strong but the corticofugal excitation is also much more pronounced. This leads to the interesting and desired effect that not only the absolute latencies but also the *latency differences* are reduced. A step towards a low opposite contrast will induce a stronger latency *reduction* than a step to a higher opposite contrast (Fig. 5). This behavior leads to more strongly reduced reaction times for weak contrasts and latency differences are leveled out.

This study is the first to implement NMDA channels in a large-scale simulation running on a parallel computer, which consists of about 15 000 cells, each of which is represented by a single processor. The major step which makes such an implementation feasible within reasonable limits of computational time is the application of the $\mathscr{Z}$-transform to define the transfer function of an NMDA channel in discrete time. The channel characteristic which obtains from our implementation reflects the measured behavior of real channels with rather high accuracy (Jones and Baughman 1988; Singer and Artola

1990). The performance of NMDA channels within the context of latency reduction, however, is limited. The reason for this is the direct inhibition from the opposing subsystems, which in our case was implemented as hyperpolarizing inhibition (reversal potential -91 mV). The hyperpolarization induced by the inhibitory connections efficiently blocks the NMDA channels (in vivo by magnesium) so that they cannot contribute to the fast depolarization required to achieve a latency reduction.

In general the question arises whether this model could be tested experimentally. In the cortex the effect of latency reduction as a consequence of the paradoxical connections is within a measurable range, but as yet it is impossible to inactivate the corticofugal feedback loop while leaving the cortex intact. To achieve this one would have to eliminate the efferent fiber system in the white matter. But unfortunately the afferent and efferent fibers are totally intermingled. In general one would require many repetitive stimulus presentations to arrive at a reliable latency distribution for an individual cell, because of the natural response variability of all (LGN and cortex) cells. To see the influence of the cortex at an LGN cell, this experiment would have to be done also during cortical inactivation, which can be achieved by cortical cooling. In the model the latency reduction observed in the LGN has a range of only a few milliseconds. While in principle it would be possible to measure this, it might nevertheless be close to the resolution limit imposed by the response variability.

Appendix. $\mathscr{Z}$-Transform of the NMDA Equation

The convolution of the main equation (5) with the input function (3) is calculated by using the $\mathscr{Z}$-transform.

First (5) is divided into its numerator $y_1(t)$ and denominator $y_2(t)$:

$$g_{\mathrm{NMDA}}(t) = y_1(t) \cdot y_2(t) \tag{A1}$$

$$y_1(t) = \hat{g} \cdot (\mathrm{e}^{-t/\tau_1} - \mathrm{e}^{-t/\tau_2}) \tag{A2}$$

$$y_2(t) = \frac{1}{1 + \eta [\mathrm{Mg}^{2+}] \mathrm{e}^{-\gamma V_\mathrm{m}}} \tag{A3}$$

This is possible because the conductance of the NMDA channel is not dependent on the history of the membrane potential V_m, but only on the time t.

This method is also used by Bernard et al. (1994), where experimental results show that the rise time is independent of the Mg^{2+} concentration (Lester and Jahr 1992; Stern et al. 1992).

Equation (8) has to be $\mathscr{Z}$-transformed. The $\mathscr{Z}$-transform of the two sums is calculated in discrete time, so that $t_n = nT$:

$$\mathscr{Z}\{y_1(nT)\} = \mathscr{Z}\{\hat{g} \cdot (\mathrm{e}^{-nT/\tau_1} - \mathrm{e}^{-nT/\tau_2})\} \tag{A4}$$

The $\mathscr{Z}$-transform of both terms is

$$\mathscr{Z}\{\mathrm{e}^{-nT/\tau_1}\} = \frac{1}{1 - \mathrm{e}^{-nT/\tau_1} \cdot z^{-1}};$$

$$\mathscr{Z}\{\mathrm{e}^{-nT/\tau_2}\} = \frac{1}{1 - \mathrm{e}^{-nT/\tau_2} \cdot z^{-1}} \tag{A5}$$

An addition in the same time domain is also an addition in the $\mathscr{Z}$ domain:

$$\mathscr{Z}\{y_1(nT)\} = y_1(z)$$
$$= \hat{g} \cdot \frac{\mathrm{e}^{-nT/\tau_1} \cdot z^{-1} - \mathrm{e}^{-nT/\tau_2} \cdot z^{-1}}{(1 - \mathrm{e}^{-nT/\tau_1} \cdot z^{-1})(1 - \mathrm{e}^{-nT/\tau_2} \cdot z^{-1})} \tag{A6}$$

In the $\mathscr{Z}$ domain a convolution of the weighted input function $x(t)$ with the numerator of the conductance function $y(t)$ is equivalent to multiplying the two functions:

$$G_1(t) = y_1(t) * x(t) \iff G_1(z) = y_1(z) \cdot x(z) \tag{A7}$$

Some conversions lead to

$$G_1(z) = \hat{g} \cdot \mathrm{e}^{-nT/\tau_2} \cdot x(z) \cdot z^{-1} - \hat{g} \cdot \mathrm{e}^{-nT/\tau_1} \cdot x(z) \cdot z^{-1}$$
$$+ [\mathrm{e}^{-nT/\tau_1} + \mathrm{e}^{-nT/\tau_2}] \cdot G_1(z) \cdot z^{-1}$$
$$- \mathrm{e}^{-nT/\tau_1} \cdot \mathrm{e}^{-nT/\tau_2} \cdot G_1(z) \cdot z^{-2} \tag{A8}$$

To get the inverse transform, the following feature of the $\mathscr{Z}^{-1}$-transform is used:

$$\mathscr{Z}^{-1}\{f(z) \cdot z^{-j}\} = f((n-j)T) \tag{A9}$$

This leads to

$$G_1(nT) = \hat{g} \cdot a_1 \cdot x((n-1)T) - \hat{g} \cdot a_2 \cdot x((n-1)T)$$
$$+ (a_1 + a_2) \cdot G_1((n-1)T)$$
$$- (a_1 \cdot a_2) G_1((n-2)T) \tag{A10}$$

with

$$a_1 = \mathrm{e}^{-nT/\tau_1} \quad \text{and} \quad a_2 = \mathrm{e}^{-nT/\tau_2} \tag{A11}$$

After a last conversion:

$$G_1(nT) = \hat{g} \cdot (a_1 - a_2) \cdot x((n-1)T)$$
$$+ (a_1 + a_2) \cdot G_1((n-1)T)$$
$$- (a_1 \cdot a_2) \cdot G_1((n-2)T) \tag{A12}$$

For calculating the absolute conductance the voltage-dependent part of (A3) is necessary, so that as main equation for the simulation of the NMDA channel we get:

$$G_{\mathrm{NMDA}}(nT) = \frac{G_1(nT)}{1 + \eta [\mathrm{Mg}^{2+}] \mathrm{e}^{-\gamma V_\mathrm{m}}} \tag{A13}$$

References

Baker FH, Malpeli JG (1977) Effects of cryogenic blockade of visual cortex on the responses of lateral geniculate neurons in the monkey. Exp Brain Res 29:433–444

Baughman RW, Gilbert CD (1980) Aspartate and glutamate as possible neurotransmitters of cells in layer 6 of the visual cortex. Nature 287:848–850

Bernard C, Ge YC, Stockley E, Willis JB, Wheal HV (1994) Synaptic integration of NMDA and non-NMDA receptors in large neuronal network models solved by means of differential equations. Biol Cybern 70:267–273

Bolz J, Rosner G, Wässle H (1982) Response latency of brisk-sustained (X) and brisk-transient (Y) cells in the cat retina. J Physiol (Lond) 328:171–190

Brettle D, Niebur E (1994) Detailed parallel simulation of a biological neuronal network. IEEE Comp Sci Eng Winter, pp 31–43

Casagrande VA, Norton TT (1991) The lateral geniculate nucleus: a review of its physiology and function. In: Leventhal A (ed) The neural basis of visual function, Vol 4. Macmillan Press. London, pp 41–84

Doetsch G (1967) Anleitung zum praktischen Gebrauch der Laplace-Transformation und der Z-Transformation. R Oldenbourg, Munich

Ferster D (1988) Spatially opponent excitation and inhibition in simple cells of the cat visual cortex. J Neurosci 8:1172–1180

Funke K, Wörgötter F (1995) Temporal structure in the light response of relay cells in the dorsal lateral geniculate nucleus of the cat. J Physiol (Lond) 485:715–737

Geisert EE, Langesetmo A, Spear PD (1981) Influence of the cortico-geniculate pathway on response properties of cat lateral geniculate neurons. Brain Res 208:409–415

Glezer VD, Tsherbach TA, Gauselman VE, Bondarko VM (1980) Linear and non-linear properties of simple and complex receptive fields in area 17 of the cat visual cortex. Biol Cybern 37: 195–208

Hubel DH, Wiesel TN (1962) Receptive fields, binocular interaction and functional architecture in the cat's visual cortex. J Physiol (Lond) 160:106–154

Jahnsen H, Llinas R (1984) Ionic basis for the electroresponsiveness and oscillatory properties of guinea-pig thalamic neurons in vitro. J Physiol (Lond) 349:227–247

Jones JP, Palmer LA (1987) The two-dimensional spatial structure of simple receptive fields in cat striate cortex. J Neurophysiol 58:1187–1211

Jones KA, Baughman RW (1988) NMDA- and non-NMDA receptor components of excitatory synaptic potentials recorded from cells in layer V of rat visual cortex. J Neurosci 8:3522–3524

Kalil RE, Chase R (1970) Corticofugal influence on activity of lateral geniculate neurons in the cat. J Neurophysiol 33:459–474

Lester RA, Jahr CE (1992) NMDA behaviour depends on agonist affinity. J Neurosci 12:635–643

Levick WR (1973) Variation in the response latency of cat retinal ganglion cells. Vision Res 13:837–853

Llinas R, Jahnsen H (1982) Electrophysiology of mammalian thalamic neurons in vitro. Nature 297:406–408

McClurkin JK, Optican LM, Richmond BJ (1994) Cortical feedback increases visual information transmitted by monkey parvocellular lateral geniculate nucleus neurons. Vis Neurosci 11:601–617

Mel B (1992) NMDA-based pattern discrimination in a modeled cortical neuron. Neural Comp 4:502–517

Montero VM (1991) A quantitative study of synaptic contacts on interneurons and relay cells of the cat lateral geniculate nucleus. Exp Brain Res 86:257–270

Montero VM (1994) Quantitative immunogold evidence for enrichment of glutamate but not asparate in synaptic terminals of retino-geniculate, geniculo-cortical, and cortico-geniculate axons in the cat. Vi Neurosci 11:675–681

Murphy PC, Sillito AM (1987) Corticofugal feedback influences the generation of length tuning in the visual pathway. Nature 329:727–729

Oppenheim AV, Schafer RW (1975) Digital-signal processing. Prentice-Hall, London

Palmer LA, Davis TL (1981) Receptive-field structure in cat striate cortex. J Neurophysiol 46:260–276

Richard D, Gioanni Y, Kitsikis A, Buser P (1975) A study of geniculate unit activity during cryogenic blockade of the primary visual cortex in the cat. Exp Brain Res 22:235–242

Sherman SM, Koch C (1986) The control of retinogeniculate transmission in the mammalian lateral geniculate nucleus. Exp Brain Res 63:1–20

Sillito AM, Jones HE, Gerstein GL, West DC (1994) Feature linked synchronisation of thalamic relay cell firing induced by feedback from the visual cortex. Nature 369:479–482

Singer W, Artola A (1990) The involvement of N-methyl-D-aspartate receptors in induction and maintenance of long-term potentiation in rat visual cortex. Eur J Neurosci 2:254–269

Stern P, Edwards FA, Sakmann B (1992) Fast and slow components of unitary EPSCs on stellate cells elicited by focal stimulation in slices of rat visual cortex. J Physiol (Lond) 428:707–722

Tolhurst DJ, Dean AF (1990) The effects of contrast on the linearity of spatial summation of simple cells in the cat's striate cortex. Brain Res 79:582–588

Troy JB, Robson JG (1992) Steady discharges of X and Y retinal ganglion cells of cat under photopic illumination. Vis Neurosci 9:535–553

Wörgötter F, Koch C (1991) A detailed model of the primary visual pathway in the cat: comparison of afferent excitatory and intra-cortical inhibitory connection schemes for orientation selectivity. J Neurosci 11:1959–1979